Chaotic Neoclassical Separatrix Dissipation in Parametric Drift-Wave Decay

A. A. Kabantsev,[1] Yu. A. Tsidulko,[2] and C. F. Driscoll[1]
[1]Department of Physics, University of California at San Diego, La Jolla, California 92093, USA
[2]Budker Institute of Nuclear Physics, Novosibirsk 630090, Russia
(Received 2 August 2013; published 7 February 2014)

Experiments and theory characterize a parametric decay instability between plasma drift waves when the nonlinear coupling is modified by an electrostatic barrier. Novel mode coupling terms representing enhanced dissipation and mode phase shifts are caused by chaotic separatrix crossings on the wave-ruffled separatrix. Experimental determination of these coupling terms is in broad agreement with new chaotic neoclassical transport analyses.

DOI: 10.1103/PhysRevLett.112.055003 PACS numbers: 52.35.Mw, 52.25.Fi, 52.27.Jt, 52.55.−s

Collisional neoclassical transport (NCT) theory [1–7] provides a baseline estimate for particle transport and energy dissipation in many applications. In collisional NCT, particles accumulate drifts from global "error fields" acting over multiple equilibrium bounce orbits, and collisions then make these drifts irreversible. This leads to bulk particle transport if the error fields are externally maintained, and leads to wave damping if the waves themselves are the error fields. Stronger transport is generally labeled "anomalous", but here we describe "chaotic" enhancements within the NCT framework.

NCT effects are particularly strong if some equilibrium orbits are bounded by electric or magnetic trapping barriers, creating distinct populations of locally trapped particles. Then, the velocity distribution function has strong distortions at the separatrix energy [2,6,7], and small changes in particle energy due to collisions can have large transport effects. In toroidal devices, the toroidal curvature provides an unavoidable error field, and trapping separatrices are ubiquitous.

Recent theory and experiments on cylindrical electron plasmas have characterized a *chaotic* variant of NCT [8–12] which is essentially *independent* of collisionality. In the simplest form of chaotic NCT, enhanced separatrix crossings arise from equilibrium plasma rotation along θ variations (ruffles) in the separatrix, giving enhanced transport. The recent experiments [8,12] utilize a $\cos(\theta - \theta_B)$ error field from a controlled magnetic tilt, and an electrostatic barrier with an applied $\cos[2(\theta - \theta_m)]$ ruffle. This produces a striking $\sin^2(\theta_B - \theta_m)$ signature for particle transport and wave damping rates, in broad quantitative agreement with chaotic NCT theory [9–11]. In toroidal stellarators, this chaotic form of superbanana transport [5] appears to be dominant in low-collisionality fusion regimes [12].

More generally, plasma waves or turbulence may also cause chaotic NCT, by modifying the separatrix or particle energies [8,9,12], and this Letter describes a parametric decay instability where the pump mode ruffles the separatrix, causing chaotic NCT dissipation. We consider the near-resonant decay instability between $E \times B$ drift (diocotron) modes: a large amplitude $m_\theta = 2$, $k_z = 0$ pump mode decays into an $m_\theta = 1$, z-antisymmetric daughter mode, with $\omega_2 \approx 2\omega_1$. Analysis of nonlinear fluid convection gives a conservative mode coupling term [13,14] which enables parametric decay and energy sloshing between modes, as commonly observed in nonlinear mechanical systems [15]. However, our prior experiments [16] showed that dissipation at the separatrix changed the nature of the energy exchange, motivating further experiments and an analysis of chaotic NCT for this process.

Chaotic NCT theory now predicts 3 new terms in the nonlinear coupling equations, causing (i) enhanced dissipation, (ii) shifts in the relative mode phases during exponential growth, and (iii) frequency shifts in the daughter mode. The present experiments characterize the first two of these terms from their effects on the exponential growth phase of the parametric decay.

The pure electron plasma columns utilized here are confined in a cylindrical Penning-Malmberg trap, as shown in Fig. 1. Electrons are confined radially by a uniform axial magnetic field $B = 3$ kG $\hat{z}$, and confined axially by voltages $V_c = -100$ V on end cylinders with wall radius $R_w = 3.5$ cm. The electron columns have length $L_p = 36$ cm and density profile $n_e(r)$ with central density $n_0 = 2.0 \times 10^7$ cm^{-3} decreasing smoothly to zero at 1.5 cm,

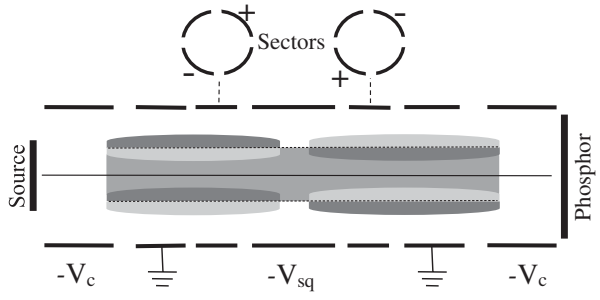

FIG. 1. Schematic of the cylindrical trap and electron plasma, with voltage $-V_{sq}$ creating an electrostatic separatrix. Density perturbations for a TPDM are also shown.

giving effective radius $R_p \equiv \sqrt{2}\langle r^2\rangle^{1/2} = 1.2$ cm. The unneutralized charge results in an equilibrium potential energy $\phi_e(r)$, and the resulting $E \times B$ drift rotation $f_E(r) \equiv cE(r)/2\pi rB$ decreases monotonically from $f_{E0} = 98$ kHz. The electrons have a near-Maxwellian velocity distribution with (approximate) thermal energy $T \approx 0.7$ eV, giving axial bounce frequency $\omega_b \equiv \pi\bar{v}/L_p = 3000/\text{ms}$ and rigidity $\mathcal{R} \equiv \omega_b/\omega_{E0} \approx 5$. The electron-electron collision rate $\nu_{ee} = 0.5/\text{ms}$ is low compared to ω_E and ω_b, so drifts accumulate over many equilibrium orbits.

A strong electrostatic trapping barrier is created by a "squeeze" voltage $V_{\text{sq}} \approx -13$ V applied to the central 3.5 cm cylinder, giving a separatrix barrier energy $\phi_{eX}(r)$ at $z = 0$. This barrier nominally traps a fraction $\eta_t(r)$ in the left or right end, while the passing fraction $\eta_p = 1 - \eta_t$ of higher-velocity electrons transit the entire length. Here, $\eta_t(0) \approx 0.2$, and $\eta_t(R_p) \approx 0.95$.

The resonant decay instability [16] studied here occurs between two electrostatic drift (diocotron) modes, with $\omega_2 \approx 2\omega_1$. These modes are easily excited and monitored by wall electrodes, with linear eigenfunctions $\Psi_m(r,\theta,z,t) = A_m(\tau)\exp(im\theta - i\omega_m t)Z(z)\psi_m(r)$, and the received wall signals $V_w(t)$ accurately determine the (complex) mode amplitudes $A_m(\tau)$, varying on the slow time scale τ. The $m = 2$ pump mode is a rotating elliptical distortion of the entire electron column, with nominally uniform $Z(z)$, having frequency $\omega_2 \approx \omega_{E0}$ and essentially zero damping. For a "square" $n(r)$ profile, the plasma edge would vary as $\delta R_p(\theta, t) = |A_2|\cos(2\theta - \Theta_2 - \omega_2 t)$.

The $m = 1$ daughter mode is a trapped particle diocotron mode (TPDM) [17,18], which is a *z-antisymmetric* variant of the standard z-symmetric $m = 1$ diocotron mode, as shown in Fig. 1. The two trapped fractions η_t in either end of the trap execute oppositely phased drift orbits around the axis with displacement A_1, and this drifting perturbation is partially Debye shielded by the passing fraction η_p. The TPDM frequency is $\omega_1 = \omega_{E0}/2$ at $V_{sq}^* = -13.$V, and a linear damping rate of $\gamma_1^{\text{coll}} \approx -2.4/\text{ms}$ arises from the collisional separatrix dissipation of the oscillating η_p current. Experimentally, controlling $\Delta V_{\text{sq}} \equiv (V_{\text{sq}} - V_{\text{sq}}^*)$ controls ω_1, and we define the detuning $\delta\omega = \omega_1 - \omega_2/2 \equiv -(2\pi) \times (1.40\ \text{kHz}/V)\Delta V_{\text{sq}}$ from the measured $\omega_1(\Delta V_{\text{sq}})$.

Figure 2 shows an example of the parametric decay when the $m = 2$ pump wave is excited to amplitude $A_2 = 1.07$ mm by a 30-cycle burst applied to the wall sectors. The $m = 1$ daughter wave then grows exponentially from noise as $A_1 \propto \exp(\Gamma_e t)$, after which the energy sloshes between modes and decreases slowly. Here, we focus exclusively on the exponential growth phase, obtaining growth rate $\Gamma_e = 7.2/\text{ms}$ for these parameters. During this exponential growth, the phase of A_1 is "locked" to the pump A_2; that is, the phase difference $\Delta\Theta_e \equiv \Theta_2 - 2\Theta_1$

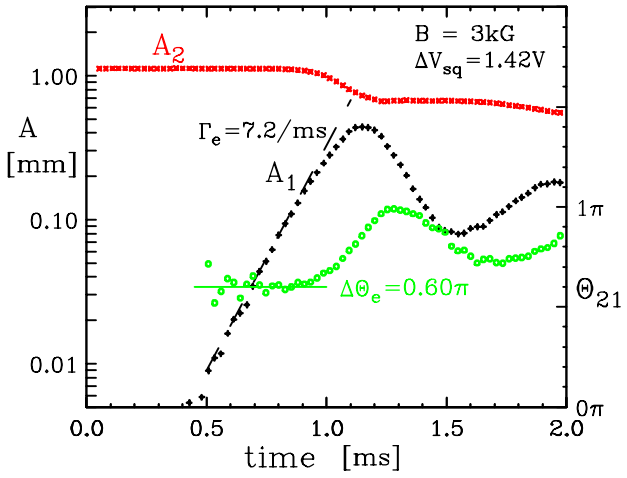

FIG. 2 (color online). Mode amplitudes A_1 and A_2 and relative phase Θ_{21} during off-resonant decay of an $m = 2$ diocotron mode into the $m = 1$ TPDM. Exponentiation rate Γ_e and locked phase Θ_{21} are obtained for detuning set by ΔV_{sq}.

is experimentally observed to be constant. Here, $\Delta\Theta_e \approx 0.60\pi$, indicating that A_1 lags behind A_2 by $\Theta_1 = 0.30\pi$.

Figures 3–5, characterize this decay instability for a range of detunings $\delta\omega$, and for a range of pump amplitudes A_2. Figure 3 shows measured growth rates Γ_e versus detuning $\delta\omega$ for 4 different pump amplitudes A_2. The growth rate decreases with detuning, as observed in Ref. [16], and the maximal detuning for which growth is observed increases with A_2. The evolution of Fig. 2 is shown as bold. The curves are theory for a single "best-fit" set of coupling parameters, as described below.

Figure 4 shows the maximal growth rate Γ_e^* versus pump amplitude A_2, with the measured collisional damping rate

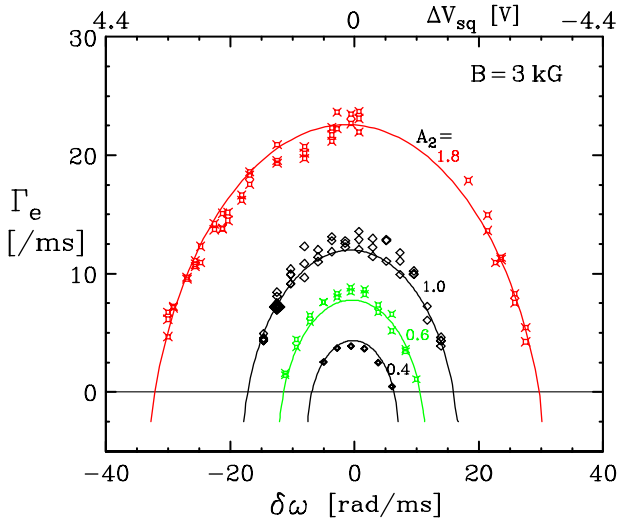

FIG. 3 (color online). Measured exponentiation rates Γ_e versus detuning $\delta\omega$ calculated from ΔV_{sq}, for 4 different pump amplitudes A_2.

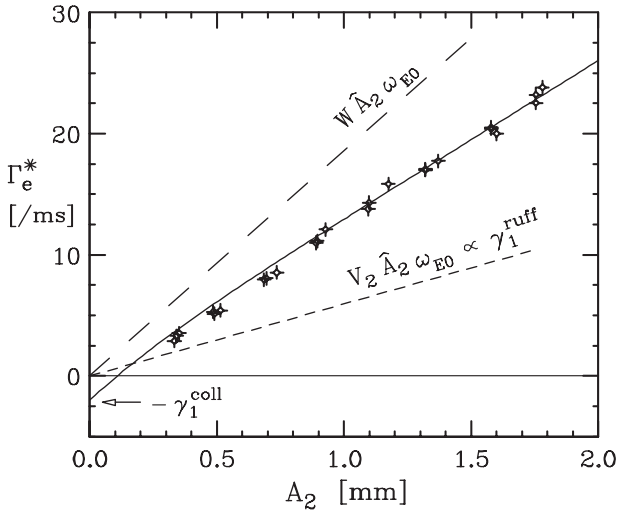

FIG. 4. Measured maximum growth rate Γ_e^* at $\delta\omega = 0$, versus pump amplitude A_2. Coupling strength WA_2 drives growth, countered by collisional damping γ_1^{coll} and ruffle-induced chaotic damping V_2A_2.

γ_1 indicated below zero. Each data point in Fig. 4 is obtained from a $\Gamma_e(\delta\omega)$ curve as in Fig. 3. A simplistic interpretation of this data (as in Ref. [16]) would be mode-coupling-induced growth at rates $0 \rightarrow 25$ dominating damping γ_1^{coll} at rate 2. However, the chaotic NCT interpretation includes ruffle-induced damping at rates $0 \rightarrow 11$ (short dashed), reducing larger coupling-induced growth at rates $0 \rightarrow 36$ (long dashed).

Finally, Fig. 5 shows the measured phase difference during exponentiation $\Delta\Theta_e \equiv \Theta_2 - 2\Theta_1$ versus detuning $\delta\omega$, for the same evolutions as in Fig. 3. In the frame of the pump mode ($\Theta_2 = 0$), the phase-locked exponentially growing mode lags behind by $\Theta_1 = \Delta\Theta_e/2$, ranging

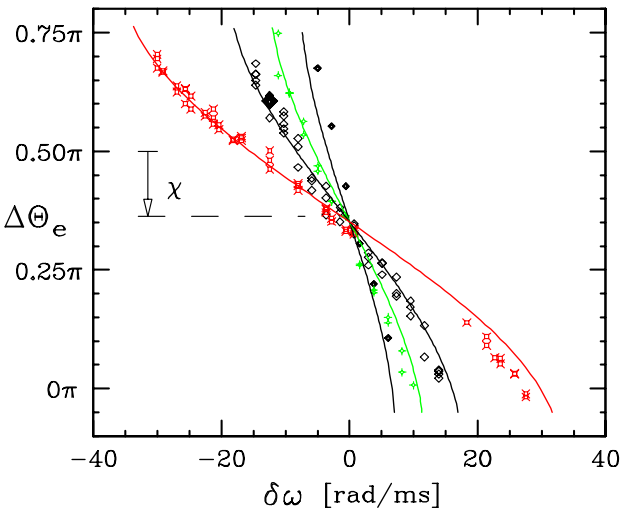

FIG. 5 (color online). Measured relative phase angle Θ_e during exponentiation for the evolutions of Fig. 3, determining $\chi = \text{atan}(V_1/V_0)$.

from $0.4\pi < \Theta_1 < 0\pi$ as $\delta\omega$ ranges from negative to positive. The functional dependence of $\Delta\Theta_e(A_2)$ is determined by the *structure* of the coupling equations, and the offset χ is given by integrals over the wave eigenfunctions. Of course, the relative phase $\Delta\Theta$ changes substantially later in the evolution, reflecting the direction of energy flow.

These measurements of Γ_e and $\Delta\Theta_e$ enable direct quantitative comparison to the nonlinear coupling coefficients predicted by chaotic NCT for a ruffled separatrix. The analysis follows the neoclassical perspective of drift displacements integrated over equilibrium trapped-particle orbits, but the novel chaotic separatrix crossings on the wave-ruffled separatrix dominate the collisional scatterings of prior analyses. Prior published theory [9–11] analyzed bounce-averaged drifts and random separatrix crossings to characterize the particle transport and TPDM damping resulting from chaotic NCT. For the present case of wave couplings, a dynamical bounce-mapping approach is being prepared for publication [19]. Here, we merely summarize the resulting *form* of the coupling equations and coefficient integrals.

For $|A_1| \ll |A_2|$, the resulting mode-coupling equations have (all real) coefficients $\{V_0, V_1, V_2, V_3\}$, as

$$\frac{d}{dt}A_2 = -\frac{\omega_{E0}}{R_w}(iV_0)A_1A_1\exp(2it\delta\omega) \tag{1a}$$

$$\frac{d}{dt}A_1 = -\frac{\omega_{E0}}{R_w}[(iV_0 - V_1)A_1^*A_2\exp(-2it\delta\omega) + (V_2 + iV_3)A_1|A_2|] - \tilde{\gamma}_1A_1. \tag{1b}$$

The theory scales with ω_{E0} and R_w, and we define the dimensionless pump amplitude $\hat{A}_2 \equiv A_2/R_w$. The damping term $\tilde{\gamma}_1 = \gamma_1^{coll}\exp(-\omega_{E0}V_2\hat{A}_2/\gamma_1^{coll})$ is an approximate form representing collisional separatrix mode damping γ_1^{coll} being suppressed exponentially by the ruffle, to be replaced by chaotic damping as $V_2\hat{A}_2$ becomes significant. The coefficients V_j depend on integrals over n_e, ϕ_e, ψ_1, ψ_2, and derivatives; the integrals are denoted by $\langle F\rangle_n \equiv \int_0^{R_w} Fn_e'dr/\int_0^{R_w} n_e'dr$. The interactions take place in a rotating frame denoted by tilde, as $\tilde{\phi} \equiv \phi - (\omega_2/2)(eB/2c)r^2$ and $\tilde{\omega}_E = \omega_E - \omega_2/2$. We obtain

$$\begin{aligned} V_0 &= G\langle(N'T/\tilde{\phi}_e')\psi_2\psi_1^2/n_e\mathcal{E}\tilde{\omega}_E\rangle_n, \\ V_1 &= G\langle g\mathcal{N}|\psi_2\psi_1^2|/n_e\mathcal{E}\tilde{\omega}_E\rangle_n, \\ V_2 &= G\langle|g|\mathcal{N}|\psi_2\psi_1^2|/n_e\mathcal{E}\tilde{\omega}_E\rangle_n, \\ V_3 &= (\pi/4)V_2. \end{aligned} \tag{2}$$

Notationally, the normalization factor is $G = \omega_{E0}R_wR_p/2\lambda_D^2$. The density profiles $N(r) \equiv n_e(\eta_p - \mathcal{E}\eta_t)$ and $\mathcal{N}(r) \equiv 4n_e e^{-y}(1+\mathcal{E})/\sqrt{\pi^3 y}$ are modified by

separatrix height $y \equiv \phi_{eX}/T$, with $\mathcal{E}(r) \equiv n_e' T/n_e \tilde{\varphi}_e'$ representing the ratio of diamagnetic and drift terms. The factor $g(r) \equiv \tilde{\phi}_{2X}/\tilde{\phi}_2 - \tilde{\phi}_{eX}'/\tilde{\phi}_e'$ characterizes the separatrix ruffle relative to the uniform regions. The radial eigenfunctions are assumed to be normalized so that $\langle(\psi_1 \omega_{E0}/\tilde{\omega}_E)^2 \eta_t\rangle_n = 1$, $\langle(\psi_2 \omega_{E0}/\tilde{\omega}_E)^2\rangle_n = 1$, and $\langle\psi_m\rangle_n > 0$.

In simplest form, this theory describes the effects of a z-localized separatrix on an otherwise z-uniform equilibrium $n_e(r)$, and radial potential profiles such as ϕ_2, ϕ_{2X}, and ψ_m are obtained from separate radial integrals. This gives the 1D coefficients of Table I. Alternately, we numerically calculate the (r, z) Boltzmann-Poisson equilibria $n_e(r, z)$ and eigenfunctions $\psi_m(r, z)$. This gives the 2D coefficients of Table I.

The exponentially growing solution of Eq. (1b) can be most simply expressed in terms of composite coupling, damping, and detuning parameters, defined by

$$W \exp(i\chi) \equiv V_0 + iV_1, \qquad D \equiv \tilde{\gamma}_1/\omega_{E0} + V_2\hat{A}_2, \qquad \Delta \equiv \delta\omega/\omega_{E0} + V_3\hat{A}_2. \tag{3}$$

The growth rate Γ_e and relative mode phases $\Delta\Theta_e$ are then given by

$$\Gamma_e/\omega_{E0} = -D + W\hat{A}_2 \cos\beta, \qquad \beta \equiv \sin^{-1}(\Delta/W\hat{A}_2), \qquad \Delta\Theta_e = \pi/2 - \chi + \beta. \tag{4}$$

The curves on Figs. 3–5, represent Eqs. (3) and (4) with the single set of 4 parameters listed in Table I as Expt. fit, using the separately measured γ_1^{coll}. These 4 parameters are a least-squares fit to a data set about twice as large as shown in Figs. 3–5, all showing similar correspondence to theory.

The two coefficients $\{V_0, V_1\}$ determine the composite coupling strength W and the "zero-detuning" phase shift $\Delta\Theta_e = \pi/2 - \chi$. The coefficient V_2 alone represents ruffle-induced damping. The coefficient V_3 predicts a ruffle-induced frequency shift not identified in these experiments, apparently due to nonlinear and apparatus-dependent shifts not included in theory. For comparison, a "simplistic" decay model with A_2-independent damping rate γ_1^{coll} and real coupling coefficient $W = V_0$ would have a linear Γ_E^* starting from γ_1^{coll} in Fig. 4, and would have zero phase offset χ in Fig. 5.

TABLE I. Exponential growth parameters from a single fit to all experimental data; and from theory Eq. (2), 1-dimension only and with R-Z potential corrections.

	W	χ	V_2/W	V_3/W
Expt. fit	1.06	0.14π	0.30	− 0.04?
1D theory	.94	0.043π	0.20	0.16
2D theory	.94	0.10π	0.32	0.25

The chaotic NCT damping $V\hat{A}_2$ is dominant in the dissipation represented by D. Prior neutral plasma NCT analyses [5] have noted that a ruffle on a separatrix can *decrease* the collisional NCT; but these analyses have not yet incorporated chaotic NCT transport and dissipation. Here, this small decrease in collisional dissipation is far outweighed by the additional ruffle-induced chaotic dissipation. On Fig. 4, the (long dashed) line labeled $W\hat{A}_2$ would be the observed growth rate without collisional damping and without the ruffle-induced dissipation represented by $V_2\hat{A}_2$ (short dashed line). Careful phasing of the global field error (wave 1) with the separatrix ruffle (wave 2) could produce a striking $\sin^2(\theta_1 - \theta_2)$ *suppression* of chaotic dissipation; but nature chooses the opposite phasing here.

We note also that the phase-independent $V_2\hat{A}_2$ contribution to the damping D of Eq. (4) agrees quantitatively with the ruffle-induced damping observed with a static or nonresonant $m = 2$ potential [9,10]. The coefficients V_1 and V_2 are closely related to integrals over the phase-dependent and phase-independent NCT diffusion coefficients $\hat{D}_1$ and $\hat{D}_0$ of Eq. (57) in Ref. [10], there obtained for a *static* ruffle. Also, we note that energy conservation requires that $V_2 > |V_1|$; this is marginally satisfied in the two theory calculations, and somewhat exceeded in the experimental fit. A phase-averaged ruffle *always* produces increased transport, corresponding to positivity of diffusion in the transport analysis.

For zero detuning, the phase angle $\Delta\Theta_e^* = \pi/2 - \chi$ of Fig. 5 and Eq. (4) determines the relative magnitudes of V_0 and V_1, as $\tan\chi = V_1/V_0$. The exponentiation analysis of Eq. (4) is only valid for $-W\hat{A}_2 < \delta\omega/\omega_{E0} < W\hat{A}_2$, with the detuning angle β varying over $-\pi/2 < \beta < \pi/2$, and we observe the 70% of this range for which $\Gamma_e > 0$. We note that these absolute phase differences between signals at different frequencies in (filtered) amplifier chains are subject to several experimental errors, so we give an uncertainty of $\pm.05\pi$ for χ.

The present experiments do not provide an unambiguous measurement of the theory coefficient V_3, because of frequency shifts not included in theory. Both drift waves show nonlinear frequency shifts at these amplitudes, with or without separatrix couplings, complicating the correspondence with the $\delta\omega$ of theory. However, the simple V_{sq}-defined $\delta\omega$ in Figs. 3 and 5 is apparently an adequate determinant of the detuning parameter β in Eqs. (3) and (4).

Other experimental uncertainties are in the (radially nonuniform) temperature $0.5 < T(r) < 1.0$ eV, the magnitude of $\omega_{E0}(\pm 10\%)$, and the calibration of A_2 ($\pm$ 10%). We note that the ratio V_2/W is independent of the ω_{E0} and A_2 calibrations; however, this still varies with T and with the details of the separatrix potentials, as suggested by the difference between the 1D and 2D calculations.

In summary, the parametric decay of drift (diocotron) waves in low-collisionality plasmas is shown to be in close agreement with predictions of chaotic neoclassical transport. Specifically, the chaotic NCT causes strongly enhanced dissipation, and determines the phase-locked mode phases during exponential growth. Similar chaotic NCT may arise from plasma rotation, waves, or turbulence in both cylindrical and toroidal plasma devices.

This work was supported by the NSF and DOE, through Grants No. PHY0903877, No. PHY0613740, and No. DE-SC0002451.

[1] A. A. Galeev, R. Z. Sagdeev, H. P. Furth, and M. N. Rosenbluth, Phys. Rev. Lett. **22**, 511 (1969).
[2] M. N. Rosenbluth, D. W. Ross, and D. P. Kostamorov, Nucl. Fusion **12**, 3 (1972).
[3] F. L. Hinton and R. D. Hazeltine, Rev. Mod. Phys. **48**, 239 (1976).
[4] P. Helander and D. J. Sigmar, *Collisional Transport in Magnetized Plasmas* (Cambridge University Press, Cambridge, England, 2002).
[5] H. Mynick, Phys. Plasmas **13**, 058102 (2006).
[6] T. J. Hilsabeck and T. M. O'Neil, Phys. Plasmas **10**, 3492 (2003).
[7] D. H. E. Dubin, Phys. Plasmas **15**, 072112 (2008).
[8] A. A. Kabantsev, D. H. E. Dubin, C. F. Driscoll, and Yu. A. Tsidulko, Phys. Rev. Lett. **105**, 205001 (2010).
[9] D. H. E. Dubin, C. F. Driscoll, and Yu. A. Tsidulko, Phys. Rev. Lett. **105**, 185003 (2010).
[10] D. H. E. Dubin and Yu. A. Tsidulko, Phys. Plasmas **18**, 062114 (2011).
[11] D. H. E. Dubin, A. A. Kabantsev, and C. F. Driscoll, Phys. Plasmas **19**, 056102 (2012).
[12] C. F. Driscoll, A. A. Kabantsev, and D. H. E. Dubin, AIP Conf. Proc. **1521**, 15 (2013).
[13] R. Z. Sagdeev and A. A. Galeev, *Frontiers in Physics* (W. A. Benjamin, New York, 1969).
[14] R. C. Davidson, *Methods in Nonlinear Plasma Theory* (Academic, New York, 1972), 6.4.
[15] A. J. Lichtenberg and M. A. Lieberman, *Regular and Chaotic Dynamics* (Springer-Verlag, New York, 1991), p. 61.
[16] A. A. Kabantsev, T. M. O'Neil, Y. A. Tsidulko, and C. F. Driscoll, Phys. Rev. Lett. **101**, 065002 (2008).
[17] A. A. Kabantsev, C. F. Driscoll, T. J. Hilsabeck, T. M. O'Neil, and J. H. Yu, Phys. Rev. Lett. **87**, 225002 (2001).
[18] Yu. A. Tsidulko, T. J. Hilsabeck, and T. M. O'Neil, Phys. Plasmas **18**, 084505 (2011).
[19] Yu. A. Tsidulko (to be published).